International Journal of Concrete Structures and Materials
Vol.18, No.3E, pp.213~219, December 2006

Experimental Determination of Concrete Fracture Properties with Modified S-FPZ Model

Jung-Heum Yon[1] and Tai-Hoon Kim[2]

(Originally published in Korean version of ***Journal of KCI***, Vol.15, No.6, December 2003)

Abstract: Modified singular fracture process zone (S-FPZ) model is proposed in this paper to determine a fracture criterion for continuous crack propagation in concrete. The investigated fracture properties of the proposed fracture model are strain energy release rate at a micro-crack tip and the relationship between crack closure stress (CCS) and crack opening displacement (COD) in the FPZ. The proposed model can simulate the actual fracture energy of experimental results fairly well. The results of the experimental data analysis show that specimen geometry and loading condition did not affect the CCS-COD relation. However, the strain energy release rate is a function of not only specimen geometry but also crack extension. The strain energy release rate remained constantly at the minimum value up to the crack extension of 25 mm, and then it increased linearly to the maximum value. The maximum fracture criterion occurred at the peak load for specimens of large size. The fracture criterion remained at the maximum value after the peak load. The variation of the fracture criterion is caused by micro-cracking and micro-crack localization. The fracture criterion of strain energy release rate can simply be the size effect of concrete fracture, and it can be used to quantify the micro-cracking and micro-crack localizing behavior of concrete.

Keywords: concrete, fracture behavior, modified S-FPZ model, fracture energy rate, fracture criterion

1. Introduction

The results of acoustic emission tests[1] show that the fracture process of concrete is initiated by the propagation of pre-existing micro-cracks or bond cracks. The size of the micro-cracking region zone depends upon the stress concentration caused by the specimen geometry and load boundary conditions.[1-4]

By increasing the load, some micro-cracks connected with and joined another, and the width of the micro-cracking zone became narrower. The decreasing width had been observed directly by scanning electron microscopy,[3,5] and it is called micro-crack localization. The peak load may be reached during the micro-crack localization. When the micro-cracking zone is stabilized at a constant width, the fracture criterion may become a constant value for incoming crack extension. During the fracture process of concrete, some tensile stress can be transferred through the micro-cracking and micro-crack bridging zone or the fracture process zone (FPZ). The tensile stress at this time is called the crack closure stress (CCS).

For the simulation of the fracture process of concrete, several fracture models have been proposed. The fictitious crack model (FCM)[6] assumes the maximum CCS as the fracture criterion, and the CCS depends upon the crack opening displacement (COD) of the assumed discrete crack. The crack band model[7] also used the maximum CCS criterion for crack extension. Nevertheless, the CCS was determined from the average strain of a constant crack band instead of a discrete crack. The two-parameter model[8] assumes an effective-elastic crack, which satisfies the measured crack tip opening displacement (CTOD) and the stress intensity factor at the peak load. The singular fracture process zone (S-FPZ) model[9] proposes a constant strain energy release rate as the fracture criterion and CCS-COD relationship for the FPZ.

Despite micro-cracking and micro-crack localization, all fracture models assume a constant fracture criterion for crack extension. The constant fracture criterion may result in the geometry and size effects, eg. the size effect model[10] using the brittleness number. The modified S-FPZ model was proposed to determine the strain energy release rate and the CCS-COD relationship of the results of three-point bending test for small size specimens. The modified S-FPZ model assumes the strain energy release rate to be a variable depending on the extent of crack extension, and the micro-cracking and localization may be simulated by using the strain energy release rate criterion.

In this study, the experimental results of two different types of specimens for the three-point bend (TPB) test[11] and the crack-line wedge-loaded (CLWL) double-cantilever beam (DCB) test[12] were applied to the modified S-FPZ model to estimate the fracture properties of the modified S-FPZ model as well as the effects of specimen geometries and loading conditions. The possible crack extensions of the TPB specimens and the CLWL-

[1] KCI member, Department of Civil Engineering, Inha University, Inchon 402-751, Korea. *E-mail: jyon@inha.ac.kr*
[2] KCI member, Department of Civil Engineering, Inha University, Inchon 402-751, Korea.

DCB specimens were 100 mm and 380 mm, respectively. The energy dissipation mechanism of propagating cracks was analyzed by the concrete fracture properties, which were estimated from the experimentally measured data of different specimen geometries and the boundary conditions.

2. Modified S-FPZ model and fracture energy

Most fracture models of concrete use a constant tensile strength or a constant critical stress intensity factor as a fracture criterion. However, analyses using the constant fracture criterion showed different results depending on the specimen geometries and loading conditions. Therefore, the modified S-FPZ model is proposed in this study to consider the localization of micro-cracking zone. In this model, the fracture properties are the same as those of S-FPZ model except that the fracture criterion is treated as a function of the crack extension.

With respect to a discrete crack, the energy dissipation mechanism of the modified S-FPZ model consists of the strain energy release rate G_I and the fracture energy rate G_{FPZ} in the FPZ. The G_I is the energy required for crack extension, and it is assumed to be a function of crack extension Δa. Additionally, the G_{FPZ} is regarded as the energy required for development of the FPZ as a function of the COD w_x. For the crack extension of Δa_i at step i, the fracture energy E_F can be calculated from the integration of the two functions $G_I(\Delta a)$ and $G_{FPZ}(w_x)$ as

$$E_F(\Delta a_i) = \int_0^{\Delta a_i} [G_I(x) + G_{FPZ}(w_x)]t dx \tag{1}$$

where, t is the thickness of a specimen at the distance x from the crack tip. From Eq. (1), the fracture energy rate G_f, which is defined as the fracture energy required for the unit area crack extension, can be calculated as the following.

$$G_f(\Delta a_i) = \frac{E_F(\Delta a_i) - E_F(\Delta a_{i-1})}{(\Delta a_i - \Delta a_{i-1})t} \tag{2}$$

The shape of COD from the CCS-COD relation should be assumed to calculate the fracture energy rate G_{FPZ}. The COD, w, at the distance x from the crack tip for the crack extension of Δa in Fig. 1 is computed by the following equation.

$$w(x) = w_x = w_o\left(\frac{x}{\Delta a}\right)^{\beta} \tag{3}$$

where, β is the shape factor, and w_o is the CTOD of the initial notch. If a linear COD along the traction free surface of the notch of a_o is assumed, the CTOD w_o can be estimated from the measured crack mouth opening displacement (CMOD, w_m) and the slope of Eq. (3) at the notch tip by the following equations:

$$\frac{dw(\Delta a)}{dx} = \beta\frac{w_o}{\Delta a} = \frac{w_m - w_o}{a_o} \tag{4}$$

$$\frac{w_o}{w_m} = \frac{1}{1 + \beta(a_o/\Delta a)} \tag{5}$$

If the difference of COD's, $\Delta w = w_1 - w_2$, between two locations of the distance Δa_w can be measured, the shape factor β can be determined by the following equation with the average slope $\Delta w / \Delta a_w$,

$$\beta = \frac{\Delta a}{\Delta a_w w_m - a_o \Delta w} \tag{6}$$

When the FPZ is developed fully or w_o is larger than the maximum COD w_c of the CCS-COD relation as shown in Fig. 1(b), the COD and the FPZ size of Δa_c can be determined by the following equations:

$$w(x) = w_x = w_c\left(\frac{x}{\Delta a_c}\right)^{\beta} \tag{7}$$

$$w_m - w_c = (a - \Delta a_c)\frac{dw(\Delta a_c)}{dx} = \beta w_c \frac{a_o + \Delta a - \Delta a_c}{\Delta a_c} \tag{8}$$

$$\frac{\Delta a_c}{a} = \frac{\beta}{w_m/w_c - (1-\beta)} \tag{9}$$

With respect to the CCS-COD relation of $f_{ccs}(w)$ and the COD of w_x, the fracture energy rate G_{FPZ} in the FPZ can be computed by the integral of the CCS-COD relation to w_x, namely,

$$G_{FPZ}(w_x) = \int_0^{w_x} f_{ccs}(w)dw - \frac{1}{2} f_{ccs}(w_x)w_x \tag{10}$$

where, the second term $\frac{1}{2} f_{ccs}(w_x)w_x$ is recoverable energy in the FPZ. If $w_x = w_c$, the fracture energy rate becomes the maximum value of $G_{FPZ}(w_c)$ or the fracture energy density defined as the fracture energy required for the full development of the unit area FPZ.

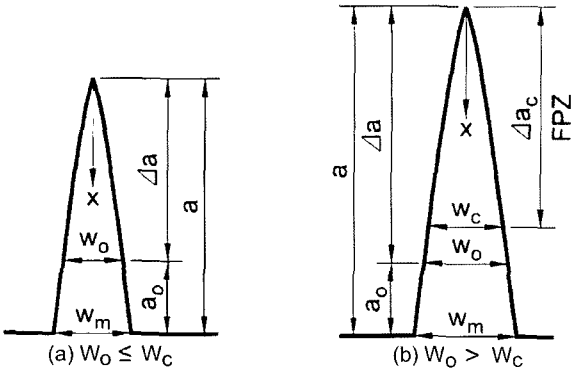

Fig. 1 Notations for crack opening shape.

3. Experimental results

The existing static fracture test results of the TPB and CLWL-DCB specimens were analyzed to determine the fracture properties of the modified S-FPZ model and to investigate the fracture behavior for different specimen geometries and loading conditions. Fig. 2 shows the geometry and the loading condition for each specimen. The geometry of the TPB specimens was 508 mm span, 127 mm depth, and 50.8 mm thickness. The TPB specimens with two different initial notch sizes of 6.4 and 25.4 mm were tested until the specimens were fractured. The notch size of 6.4 mm was equal to the maximum aggregate size.

The CLWL-DCB test setup was designed for the measurement of large crack extension of 381 mm for the effective usage

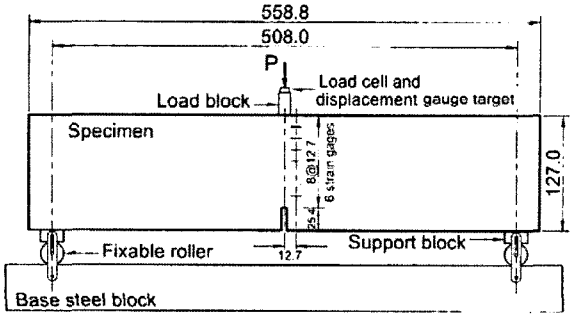

(a) TPB specimen[11]

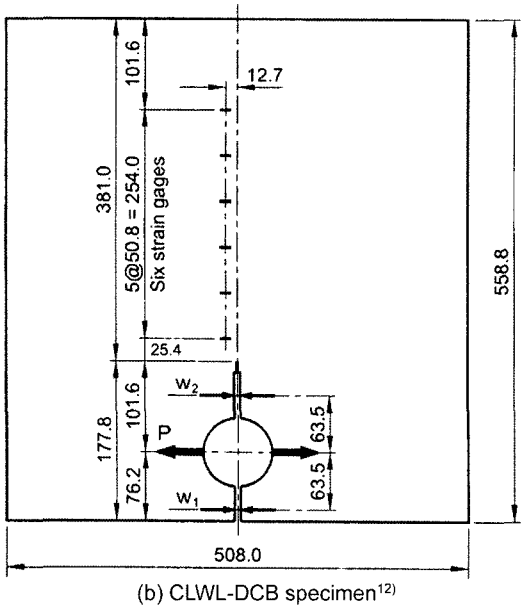

(b) CLWL-DCB specimen[12]

Thickness = 50.8 mm Unit : mm

Fig. 2 Configurations of TPB and CLWL-DCB specimens.

of the loading system. The vertical movement of a wedge was transferred to horizontal displacement of the specimen by the split-pins. The average compressive and splitting strengths of both specimens, which were cast from the same batch, were 45.9 MPa and 3.93 MPa, respectively. More detailed test setup and material properties can be found from the references 11 and 12.

The experimental results of three specimens for each TPB and CLWL-DCB tests are shown in Table 1. Fig. 3 is the measured load versus load-points displacement relations. The external work W_i at the load-point displacement δ_i was calculated by

Table 1 Results of experimental tests.[11,12]

Notch size	Test no.	Duration (sec)	Peak load (kN)	Work (N · m)	G_F (N/m)
6.4 mm	TPB001	2,070	3.817	0.840	137
	TPB002	1,260	3.277	0.551	90
	TPB003	1,410	3.237	0.625	102
	Ave.	1,580	3.444	0.672	110
25.4 mm	TPB101	2,040	3.040	0.524	102
	TPB102	1,980	2.976	0.622	121
	TPB103	1,840	2.867	0.590	114
	Ave.	1,953	2.961	0.579	112
117.8mm	DCB101	1,360	10.61	4.025	208.0
	DCB102	1,310	10.03	4.307	222.6
	DCB103	1,230	11.35	3.748	193.6
	Ave.	1,300	10.66	4.027	208.1

Note : G_F = the average fracture energy density

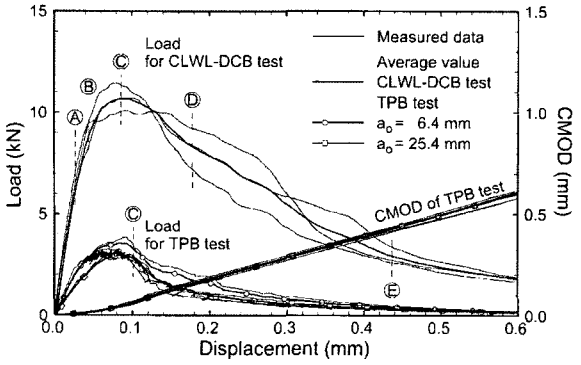

Fig. 3 Measured load versus load-point displacement relations.[11,12]

integrating the measured load versus displacement relation to δ_i, namely,

$$w_i = \int_0^{\delta_i} P d\delta \simeq \frac{1}{2}\sum_{j=1}^{i}(P_{j+1}+P_j)(\delta_{j+1}-\delta_j) \tag{11}$$

The external works in Table 1 were the values measured at the failure. The average loads in Fig. 3 were the rates of the average external work W_i^{ave} to the loading-point displacement as given by the following equation.

$$P_i^{ave} = \frac{dw_i^{ave}}{d\delta_i} \simeq \frac{w_i^{ave} - w_{i-1}^{ave}}{\delta_i - \delta_{i-1}} \tag{12}$$

Therefore, the average loads in Fig. 3 are the loads satisfying the measured external works. The average fracture energy densities of G_F^{ave} were calculated by the following equation.

$$G_F^{ave} = \frac{[\text{External work}]}{[\text{Area of critical section}]} \tag{13}$$

It can be seen from figure 3 that the CMOD's of the TPB tests with the initial notch sizes of 6.4 mm and 25.4 mm were similar. Fig. 4 shows the crack extension measured with the strain gages illustrated in Fig. 2. The crack extension rate from the TPB tests decreased suddenly after step Ⓒ, but crack extension of CLWL-DCB tests was parabolic to the load-point displacement.

Figs. 5~7 are the energy partitions calculated from the average load versus load-point relations excluding the permanent deformation, which occurs upon unloading. In this case, the recoverable strain energy is $E_{si}^{ave} = \frac{1}{2}P_i^{ave}\delta_i$, and the fracture energy E_{Fi} can be estimated from the energy balance as the

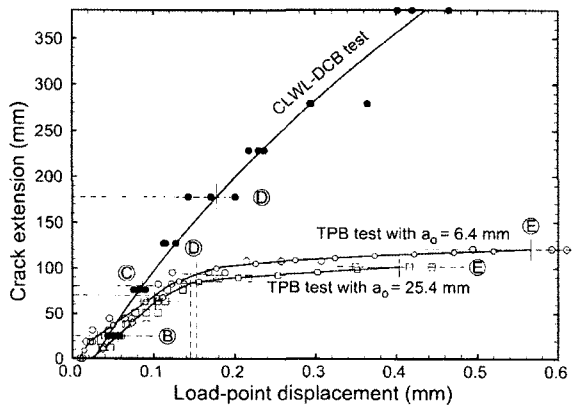

Fig. 4 Measured and average crack extensions.[11,12]

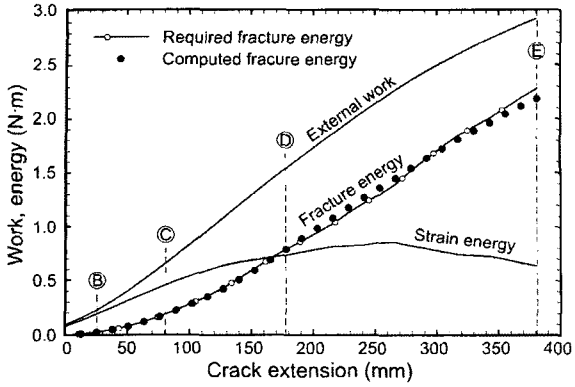

Fig. 5 Energy partitions of CLWL-DCB tests.

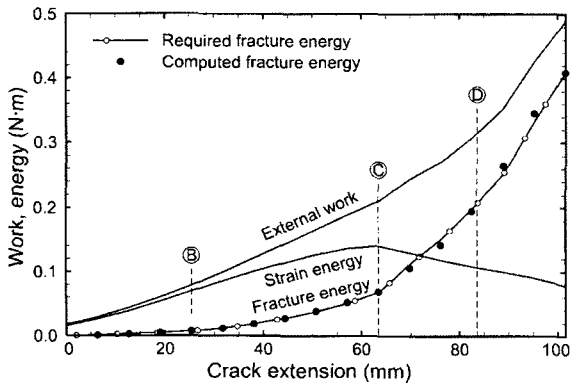

Fig. 6 Energy partitions of TPB tests (a_0 = 25.4 mm).

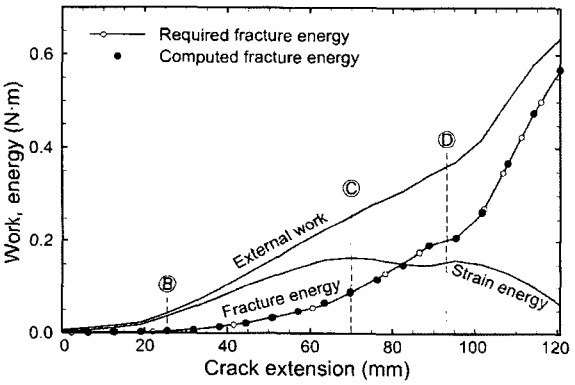

Fig. 7 Energy partitions of TPB tests (a_0 = 6.4 mm).

following.

$$E_{Fi}^{ave} = W_i - \frac{1}{2} P_i^{ave} \delta_i \tag{14}$$

The fracture energy given by Eq. 14 is the minimum value of possible fracture energies, and it can be used conservatively. The plastic deformation of concrete is not proven clearly, and the permanent deformation during unloading may be caused by the particle movement and the tortuous crack surfaces. The permanent deformation causes compressive and tensile residual stresses on the crack faces and in front of the crack tip, respectively, and then some strain energy remains in the specimen. Therefore, the dissipation energy for the permanent deformation was assumed to be equal to the strain energy caused by the residual stresses.[13]

4. Fracture properties

In order to apply the modified S-FPZ model, two fracture properties of the energy release rate G_I, the fracture energy rate G_{FPZ} in the FPZ, and the shape factor for each crack extension should be known. However, the fracture properties can not be measured directly from experimental tests. Thus, the fracture properties were determined in this study by minimizing the following standard error (SE) of the fracture energy calculated by using Eq. (1) and the required fracture energy of Eq. (14).

$$SE(\%) = \sqrt{\frac{1}{N-2} \sum_{i=1}^{N} \left[\frac{E_{Fi}^{ave} - E_f(\Delta a_i)}{E_{Fi}} \right]} \tag{15}$$

The CCS-COD relation of $f_{ccs}(w)$ was assumed to be a constant function in this study, but the strain energy release rate G_I and the shape factor β were regarded as variables of crack extension. The fracture parameters were determined by the following procedure.

① Assume a function of the strain energy release rate $G_I(\Delta a)$
② Assume the CCS-COD relation $f_{ccs}(w)$ in the FPZ
③ Calculate fracture energy rate $G_{fpz}(\Delta a_i)$ dissipated for the FPZ development during each crack extension Δa_i
④ Calculate the fracture energy E_F from Eq. (1)
⑤ Calculate the SE of Eq. (15)
⑥ If the SE is small enough, finish the procedure
⑦ Derive a function of the energy release rate $G_I(\Delta a)$ with the least square method for each crack extension Δa_i, and start over from step ②

The shape factor β of the CLWL-DCB specimen can be determined from the measured COD by Eq. (6). The shape factors of the TPB specimens should be determined by using the same procedure as that for the energy release rate.

Figs. 8~10 show the finally determined fracture properties. The fracture energies in Figs. 5~7 were calculated by Eq. (1) with these fracture properties. The standard error of the fracture energies was less than 3 percents.

The shape factors of the TPB tests in Fig. 8 were determined by the same procedure as that for the energy release rate, while the shape factors of the CLWL-DCB tests were calculate from Eq (6). The shape factor of the CLWL-DCB specimens increased slowly, and its value was less than that of the TPB specimens. Fig. 8 also shows that the initial notch size a_o of the TPB specimen affected the fracture properties. The shape factor less than 1.0 occurs when singularity exists at the crack tip. The

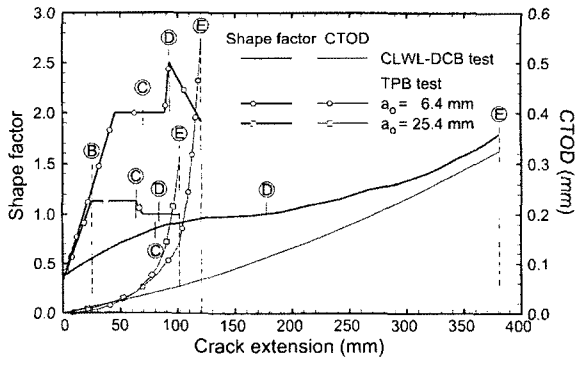

Fig. 8 Determined shape factors and CTOD's.

CTOD's in Fig. 8 were calculated by Eq. (5) with these shape factors. The CTOD's of the TPB specimens increased suddenly after the crack extension of 50 mm.

The optimized energy release rates used as the fracture criterion for the extension of a crack are shown in Fig. 9 and are listed in Table 2. Before the 25.4 mm crack extension at Step ○B , the initial energy release rate was the constant minimum value $G_{I\min}$. Afterwards, it increased linearly with the crack extension up to Step Ⓒ. After Step Ⓒ, the energy release rate remained at the constant maximum value $G_{I\max}$.

The loads and load-point displacements at Step Ⓒ are marked in Fig. 3. Step Ⓒ of the CLWL-DCB tests occurred at the peak load clearly, but that of the TPB tests occurred after the peak load and at the maximum strain energy as shown in Figs. 6 and 7. The maximum strain energy release rate at Step Ⓒ was proportional to the size of the FPZ Δa as given by following equation.

$$G_{I\max} = (2.03\ \text{N/m}^2)\Delta a - (109\ \text{N/m}) \quad (16)$$

The constant minimum strain energy release rate $G_{I\min}$ at Step Ⓑ may require pre-existing micro-crack extensions around the initial notch tip. The increasing energy release rate between Steps Ⓑ and Ⓒ can be explained by the increased stress concentration due to the micro-crack bridging and localizing. The results of acoustic emission tests[1] and scanning electron microscopy observation[5] show the same fracture procedure.

Fig. 10 shows the CCS-COD relations obtained through the applied modified S-FPZ model of this study, and the maximum CCS f_{ccso} and the critical COD w_c are listed in Table 2. The optimized CCS-COD relations in this study were compared with those of the S-FPZ model in Fig. 10, using a constant strain energy release rate and the fictitious crack model with a constant tensile strength as a fracture criterion.[13]

The f_{ccso} of the S-FPZ model with G_I= 8.74 N/m was 1.93 MPa. The maximum CCS f_{ccso} was constant until the peak load, and then it decreased suddenly after the peak load. Since f_{ccso} was used as a fracture criterion for the case of the fictitious crack model, the of f_{ccso} 3.48 MPa was a relatively large value to satisfy the measured fracture energy, but it decreased rapidly with increasing COD. After the 0.03 mm crack extension, the CCS-COD relation was similar to that of the S-FPZ model. The results of the direct tensile test[14] were also similar to that of the fictitious crack model.

The f_{ccso} of the modified S-FPZ model, in which the crack extension or the size of the FPZ was considered to be the

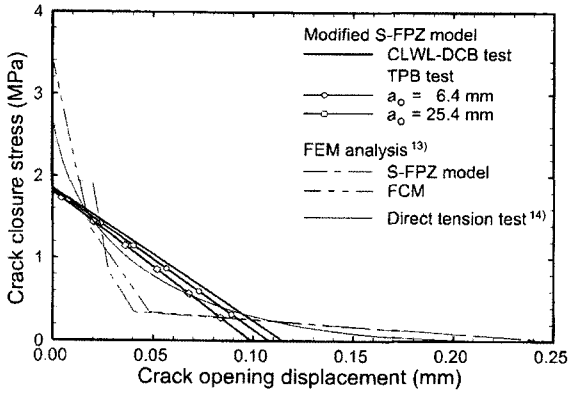

Fig. 10 Applied CCS-COD relations for FPZ.

Table 2 Applied fracture properties.

Property	TPB test		CLWL-DCB test
	6.4 mm	25.4 mm	
f_{ccso} (MPa)	1.83	1.81	1.85
w_c (mm)	0.108	0.099	0.115
G_{FPZ} (N/m)	98.8	89.8	106.5
$G_{I\min}$ (N/m)	0.771	1.93	10.61
$G_{I\mix}$ (N/m)	23.64	9.11	44.24

Note: f_{ccso} = maximum crack closure stress

fracture criterion, was 1.83 MPa, and it decreased linearly to the limit COD w_c of 0.11 mm. The simple linear relation was optimized in this study, because more complicate functions can not further decrease the standard error of the required fracture energy from the experimental tests. The CCS-COD relations of the modified S-FPZ model in Fig. 10 were very similar despite the different specimen geometries and loading conditions.

5. Fracture behaviors according to modified S-FPZ model

The standard error of the computed fracture energies with the fracture properties in Figs. 8~10 to the measured ones in Figs. 5~7 was less than 3 percents. Using the properties shown in Figs. 8~10, the computed fracture resistance or the fracture energy rate G_f, which is defined as the energy required for extension and development of unit area FPZ, is shown in Fig. 11. The resistance was computed from the following equation.

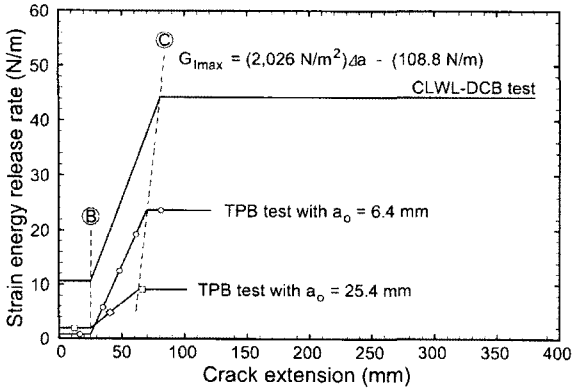

Fig. 9 Applied strain energy release rates.

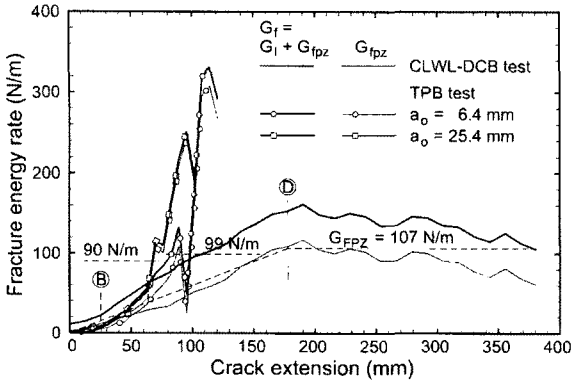

Fig. 11 Computed resistance curves.

$$G_f = G_I + G_{fpz} \tag{17}$$

where, G_I is the function of the strain energy release rate of the crack extension Δa_i as shown in Fig. 9, and the G_{fpz} required for development of the FPZ was computed by the following equation.

$$G_{fpz}(\Delta a_i) = \frac{E_{FPZ}(\Delta a_i) - E_{FPZ}(\Delta a_{i-1})}{(\Delta a_i - \Delta a_{i-1})t} \tag{18}$$

where, the E_{FPZ}, which is dissipated energy for development of the FPZ during crack extension Δa_i, is the same value as the second term of Eq. (1), and it can be calculated by integrating the CCS-COD relation in Fig. 10 as expressed mathematically by the following equation.

$$E_{FPZ}(\Delta a_i) = \int_o^{\Delta a_i} G_{FPZ}(w_x) t dx \tag{19}$$

Prior to the maximum strain energy release rate at Step Ⓒ in Fig. 9, the resistances of the TPB specimens were very similar, and then they increased suddenly after Step Ⓒ. The decreasing rate of crack extension in Fig. 4 and increasing rate of the CTOD in Fig. 8 show that more energy dissipates for development of the FPZ rather than for crack extension after Step Ⓒ.

Prior to Step Ⓒ, the fracture resistance of the CLWL-DCB specimens was larger than those of the TPB specimens due to the larger initial strain energy release rate in Fig 9. However, the fracture resistance of the CLWL-DCB specimens increased linearly with the crack extension up to Step Ⓓ. After Step Ⓓ, the resistance of the CLWL-DCB specimens was roughly a constant value of the limit fracture energy rate. The different resistances of the TPB and CLWL-DCB specimens may be caused by the crack arresting after the unstable crack propagation in the TPB specimens and different energy dissipation rates in crack extension and development of the FPZ.

Fig. 12 shows the size of the FPZ, and Step Ⓓ is defined when the FPZ is developed fully. The FPZ sizes of the TPB specimens decreased rapidly after Step Ⓓ, since larger energy dissipated owing to the increased COD in the FPZ rather than crack extension. The FPZ size of the CLWL-DCB specimens remained roughly constant after Step Ⓓ. The unstable crack extension at Step Ⓒ and the crack arresting at Step Ⓓ of relatively small size specimens can be obtained from the measured CTOD's in Fig. 8 and the computed FPZ sizes in Fig. 12. The crack extension Δa and the load-point displacement u_p for each step of this study are listed in Table 3.

The amount of singularity can be expressed by the singularity rate (SR) defined as the ratio of the strain energy release rate to the fracture energy rate as expressed by the following equation and is shown in Fig. 13.

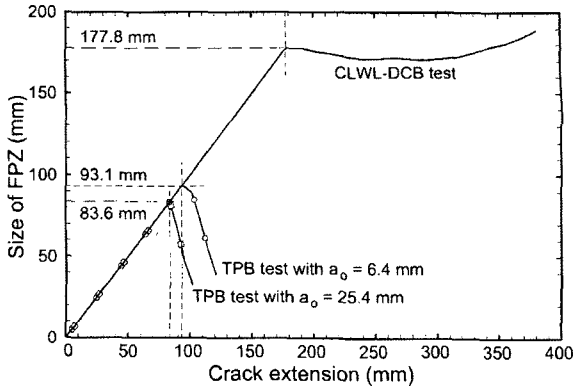

Fig. 12 Computed sizes of FPZ and crack extensions at step Ⓓ.

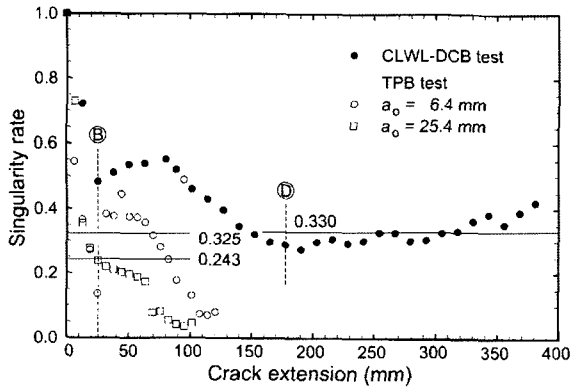

Fig. 13 Singularity rates for crack extensions.

$$SR = \frac{G_I}{G_f} = \frac{G_I}{G_I + G_{fpz}} \tag{20}$$

In Eq. (20), SR = 1 for the linear elastic fracture mechanics (LEFM) and SR = 0 for the fictitious crack model. The singularity rates of the TPB specimens deceased continuously as shown in Fig. 13, and the decreasing rate was more conspicuous with smaller initial notch size. In spite of the clear evidence of singularity in large specimens, the singularity rates of the TPB specimens decreased to 0.1 after Step Ⓒ. The singularity rate of the CLWL-DCB specimens decreased with increasing FPZ, and it reached roughly a constant value of 0.33 at Step Ⓓ, at which point the FPZ was developed fully.

6. Conclusions

The modified S-FPZ model, which can assess the variation of a fracture criterion with crack extension, is proposed in this paper. Two fracture properties, the strain energy release rate and

Table 3 Crack extension and load-point displacement at each step. (unit: mm)

Step	TPB test				CLWL-DCB test		Expected behavior
	a_o = 6.4 mm		a_o = 25.4 mm				
	Δa	u_p	Δa	u_p	Δa	u_p	
Ⓐ	0.0	0.0085	0.0	0.024	0.0	0.027	Micro-cracking
Ⓑ	25.4	0.031	25.4	0.056	25.4	0.044	Micro-crack localizing
Ⓒ	69.9	0.101	63.5	0.102	80.7	0.086	Maximum fracture criterion
Ⓓ	93.1	0.153	83.6	0.145	177.8	0.178	Full development of FPZ
Ⓔ	120.7	0.566	101.6	0.403	381.0	0.437	Maximum crack extension

the CCS-COD relation, are applied in this model. The strain energy release rate was the fracture criterion depending on the crack extension. The proposed model could simulate the experimental results of continuously propagating crack with the standard error of less than 3 percents.

The following conclusions on the fracture behavior of the concrete, which was investigated by the modified S-FPZ model, are obtained.

1) The CCS decreased linearly with the COD, and the CCS-COD relation was not so much affected by the specimen geometries and loading conditions.

2) The energy release rate as a fracture criterion was a constant minimum value $G_{I\min}$ up to the crack extension of 25 mm. Afterwards, the energy release rate increased linearly with the crack extension, and it reached the maximum value $G_{I\max}$ at the peak load for the CLWL-DCB specimens and at the maximum strain energy for the TPB specimens, respectively.

3) The constant $G_{I\min}$ and the increasing G_I compared to the constant $G_{I\max}$ may be caused by micro-crack extension and localization of micro-cracking area, respectively. Based on the experimental data, the variation of the G_I can be used for quantitative analysis of micro-crack localization.

4) The specimen geometries and loading conditions affect the fracture criterion of the strain energy release rate only, and it can be simplify the size effects.

5) If the specimen size is large enough, the fracture resistance reaches a constant limit value after the full development of the fracture process zone, and the strain release rate required for crack extension was 1/3 of the total fracture energy rate. It is very difficult to determine the fracture properties of relatively small size specimens due to unstable crack propagation and crack arresting.

Acknowledgements

This research was supported by the inha university Research Grant. The financial support is gratefully acknowledged.

References

1. Landis, E. and Shah, S. P., "Recovery of microcrack parameter in mortar using quantitative acoustic emission," *Journal of Nondestructive Evaluation*, Vol.12, No.4, 1993, pp.213~232.

2. Li, Z., Kulkarni, S. M., and Shah, S. P., "New test method for obtaining softening response of unnotched concrete specimen under uniaxial tension," *Experimental Mechanics*, Vol.33, No.3, 1993, pp.181~188.

3. Li, Z., "Microcrack characterization in concrete under uniaxial tension," *Magazine of Concrete Research*, Vol.48, No.176, 1996, pp.219~228.

4. Li, F. and Li, Z., "Acoustic emission monitoring of fracture of fiber reinforced Concrete in tension," *Material Journal*, ACI, Vol.97, No.6, 2000, pp.629~636.

5. Krstulovic Opara, N., "Fracture process zone presence and behavior in mortar specimens," *Material Journal*, ACI, Vol.90, No.6, 1993, pp.618~626.

6. Hillerborg, A., Modeer, M., and Petersson, P.-E., "Analysis of crack formation and crack growth in concrete by means of fracture mechanics and finite elements," *Cement and Concrete Research*, Vol.6, No.6, 1976, pp.773~782.

7. Bazant, Z. P. and Oh, B. H. "Crack band theory for fracture of concrete. Materials and Structures," *RILEM*, Vol.16, 1983, pp.155~177.

8. Jenq, Y. S. and Shah, S. P., "A two parameter fracture model for concrete," *Journal of Engineering Mechanics*, ASCE, Vol.111, No.4, 1985, pp.1227~1241.

9. Yon, J.-H., Hawkins, N. M., and Kobayashi, A. S., "S-FPZ model for concrete SEN specimen," *Fracture mechanics of concrete structure*, Elsevier Applied Science, London, England, 1992, pp.208~213.

10. Bazant, Z. P. and Kazemi, M. T., "Determination of fracture energy, process zone length and brittleness number from size effect, with application to rock and concrete," *International Journal of Fracture*, Vol.44, 1990, pp.111~131.

11. Yon, J.-H., "Resistance Curves of Propagating Cracks for Concrete Three-Point Bend Specimens," *Journal of the Korea Concrete Institute*, Vol.13, No.6, 2001, pp.568~574.

12. Yon, J.-H., "Resistance Curves of Concrete CLWL-DCB Specimens," *Journal of the Korea Concrete Institute*, Vol.14, No.3, 2002, pp.357~364.

13. Yon, J.-H., Hawkins, N. M., and Kobayashi, A. S., "Comparisons of concrete fracture models," *Journal of Engineering Mechanics*, ASCE, Vol.123, No.3, 1997, pp.196~203.

14. Navalurkar, R. K., Hsu, C. T. T., Kim, S. K., and Wecharatana, M., "True Fracture Energy of Concrete," *Materials Journal, ACI*, Vol.96, No.2, 1999, pp.213~225.